ENPH 455/555 Final Report

Design of a

Photonic Crystal Ring Resonator System

to

Produce Squeezed Light

by

A. Fullerton

A thesis submitted to the

Department of Physics, Engineering Physics, and Astronomy

in conformity with the requirements for

the degree of Bachelor of Applied Science

Queen's University

Kingston, Ontario, Canada

April 2024

Abstract

As classical digital computers approach their limitations, there is growing interest in practical quantum computing due to its potential to solve previously intractable problems. This report focuses on enhancing the generation of entangled squeezed states, which have fundamental applications in quantum computing. We explore the utilization of micro ring resonators (MRRs), specifically investigating a more compact design formed from coupled cavities in a photonic crystal slab. By leveraging the ability of MRRs to amplify light intensity, this project aims to generate entangled squeezed states through a nonlinear optical process called spontaneous four-wave mixing (SFWM) in which a single state of light splits into two child states called the signal and idler states. Through the implementation of simulations in Lumerical and MATLAB, various configurations of coupled-cavity ring resonators were explored, emphasizing optimization of frequency spacing, nonlinear mode overlap and quality factor. Ring performance was examined under controlled variations in ring size and defect cavity radius. The most optimal configurations were found to be ones in which the signal and idler frequencies were equally spaced around the pump frequency which sat at the inflection point of the dispersion relation for the modes given by a tight binding model. Notably, a uniformly doubly spaced 24-cavity ring with a defect radius of 100 nm emerged as the most promising design, demonstrating favorable mode frequency spacing and achieving a 6.31% nonlinear mode overlap efficiency. Further experimentation with ring configurations of varying ring size and cavity defect size is essential for optimizing the design and realizing practical viability.

Table of Contents

List of Tables

List of Figures

1 Problem Objective

As we reach the limitations of classical digital computers, interest in developing practical quantum computers is ever increasing. Research has found that quantum computers can solve problems that no classical computer can solve in any feasible amount of time, making them incredibly powerful [1]. Such computers generally rely on the quantum entanglement of two or more states to operate. These form the fundamental components of quantum computing, called qubits.

An exciting new avenue to produce qubits for computation is by using a pair of entangled squeezed states. Photons adhere to an uncertainty principle which states that one cannot simultaneously know the values of two conjugate observables (e.g. position and momentum) of a quantum system, with perfect accuracy. A squeezed state is one in which the uncertainty in one property is reduced (squeezed) at the expense of the certainty of the conjugate property [2] (See Appendix B).

Squeezed light can be generated using nonlinear optical processes accessible under high-intensity illumination. This includes a process called spontaneous four-wave mixing (SFWM), which can occur when a laser (the pump) interacts with a nonlinear crystal. In this interaction, photons from the laser incident on the crystal are converted to pairs of correlated signal and idler photons [3]. This squeezing of the phase uncertainty allows for the precision required for accurate measurements in quantum computing.

Enhanced generation of entangled squeezed states can be achieved through the utilization of a micro ring resonator (MRR). An MRR is characterized by a curved waveguide closed onto itself, thereby forming a resonant cavity. Proper configuration of the MRR enables the coherent buildup of intensity, significantly enhancing its nonlinear response [4]. A ring resonator-like structure can be formed from defects in a lattice of airholes on a photonic crystal slab. When side-coupled to a straight coupled-cavity waveguide (CCW), this can serve as a compact generator for squeezed light. Table 1 provides an overview of the advantages of both waveguide and coupled-cavity MRR’s. This project aims to explore the potential of implementing a coupled-cavity ring resonator system for generating squeezed light.

Table 1 A comparison of coupled-cavity and waveguide MRRs.

Coupled-Cavity MRR	Waveguide MRR
Smaller radius	Larger radius
Lower quality factor	Higher quality factor
Potentially sensitive to fabrication variations	Simplified fabrication
Tougher to couple for efficient optical signal transfer	Good phase matching
Higher nonlinear interaction	Lower nonlinear interaction

2 Background

Designing such a solution requires an understanding of elements of non-linear optics, the tight binding model, and optical microresonators.

2.1 Coupled Cavity Waveguides

This design implements a coupled-cavity waveguide (CCW) on a photonic crystal (PC). Defect-free PC slabs are periodic dielectric structures that can manipulate the flow of light in a manner similar to how electronic band gaps manipulate the flow of electrons in semiconductors. Just like electronic band gaps, photonic band gaps are ranges of frequencies where light cannot propagate through the PC [5]. One may form single-defect cavities in the PC slab by removing or shrinking an air hole at a particular lattice site, and thus locally disrupting the periodicity of the structure. This forms a localized single defect cavity mode in which the resonant frequency lies within the

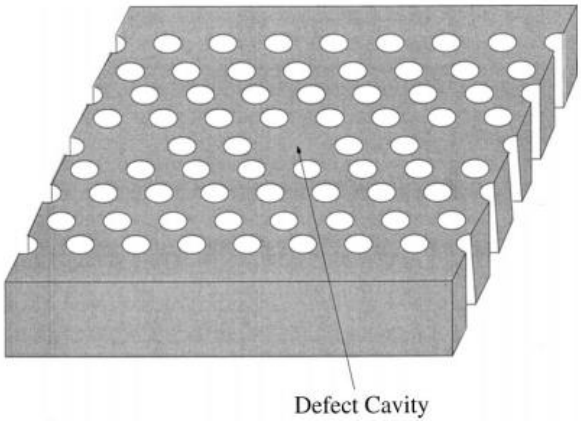

Figure 1 A coupled-cavity waveguide implementation on a photonic crystal slab [13].

transverse electric (TE) photonic band gap of the PC slab. By coupling these defect cavities, the resonant frequency is allowed to propagate through the PC slab akin to a waveguide [5]. The implementation of a CCW on a PC slab is shown in Figure 2. This serves as our photonic guidance architecture.

The dispersion relation for the resonant frequencies in the CCW can be calculated using the tight binding (TB) model, a modeling approach that focuses on the interactions between states on adjacent lattice sites within a crystal structure. The dispersion relation in a nearest-neighbor tight binding (NNTB) model is given by [6]:

$$\omega_m = \omega_o - \frac{\Delta}{2}\cos(k_m d) \tag{1}$$

Where Δ corresponds to the width of the photonic band, d is the distance between cavities in the lattice and k_m is given by:

$$k_m = \frac{2\pi m}{Nd} \tag{2}$$

Where N is the number of cavities in the ring and m is an integer such that:

$$-\frac{N}{2} < m < \frac{N}{2} \tag{3}$$

The dispersion relation for the resonant modes using NNTB is illustrated in Figure 3 where the dots represent the resonant modes in the ring.

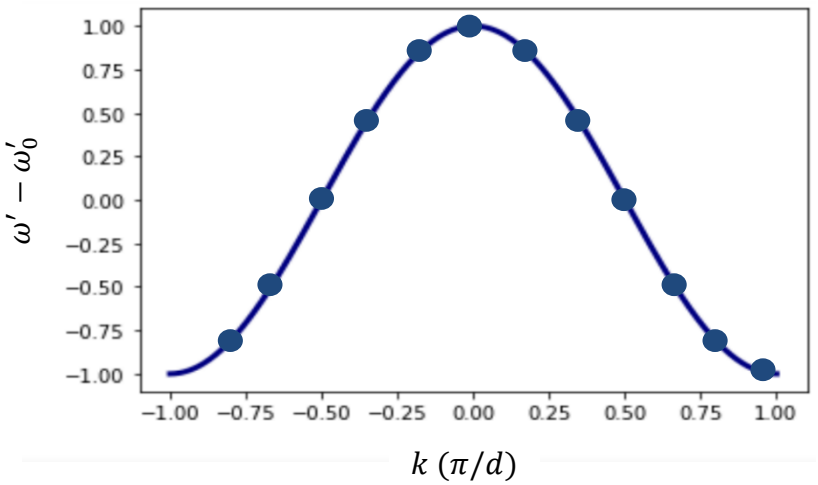

Figure 2 An illustration depicting a dispersion relation for a coupled-cavity ring where the dots represent the resonant frequencies.

Note that the symmetry exhibited by the dispersion relation should lead to pairs of equal frequencies with opposite sign wave vectors for all but the frequencies at either peak of the curve. This behavior may experience slight disruption for expansions beyond NNTB, but a similar pattern is expected to be maintained.

2.2 Spontaneous Four-Wave Mixing

For a given material in the presence of weak electric fields, a linear response is observed, however for strong laser fields, non-linear interaction can be observed. In a non-dispersive, nonlinear medium, the polarization due to a strong laser field can be expressed as:

$$\tilde{P}(t) = \epsilon_o[\chi^{(1)}\tilde{E}(t) + \chi^{(2)}\tilde{E}(t)^2 + \chi^{(3)}\tilde{E}(t)^3 + \cdots] \quad (4)$$

where the χ's are the electrical susceptibility at different orders and ϵ_0 is the permittivity of free space [2]. When a laser is incident on a crystal lattice structure whose third-order susceptibility is nonzero, a sufficiently intense field excitation enables a quantum process which generates entangled states of light. Under a third-order process, called spontaneous four-wave mixing (SFWM), a single state of light splits into two child states called the signal and idler states. This non-linear optical process enforces the following constraint on the frequencies [5]:

$$2\omega_p = \omega_s + \omega_i \quad (5)$$

Where $\omega_{p,s,i}$ represent the frequencies of the pump, signal, and idler waves respectively, and $\omega_s > \omega_i$. Since these frequencies are complex in a lossy coupled-cavity photonic crystal system, they are represented by:

$$\omega = \omega' + j\omega'' \quad (6)$$

This process is maximally efficient when the states are completely phase matched such that:

$$2k_p = k_s + k_i \quad (7)$$

Where $k_{p,s,i}$ are the wave vectors for associated with each electromagnetic wave.

SFWM from a third-order crystal is shown in Figure 3 as well as the relationship of the signal and idler frequencies, as well as their wave vectors, with those of the pump. These relationships satisfy conservation of energy and conservation of crystal momentum.

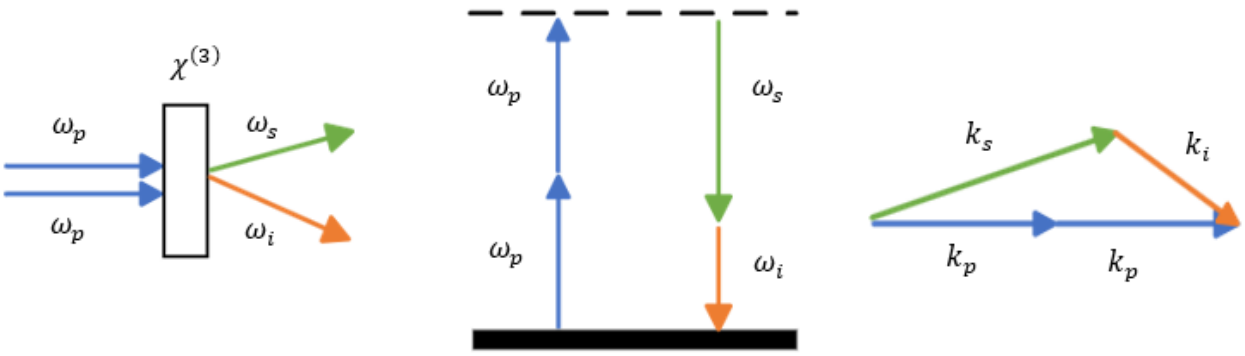

Figure 3 An illustration of the relationships between the pump, signal, and idler states for SFWM.

2.3 Micro Ring Resonators

The design for this project is based on that of a ring waveguide side-coupled to a channel such that the pump can propagate into the ring and build up intensity relative to the channel allowing for enhanced generation of entangled states of light [1]. The CCW can be coupled with a cavity system motivated by the structure of a micro ring resonator (MRR) as shown in Figure 4 [1]. Like the MRR, this can be configured resonantly with the channel to amplify the light intensity. This configuration can provide a compact source of non classical light that can be integrated into a chip for quantum computing [1]. Inside the resonator exists only a discrete set of resonant frequencies which can be amplified [4].

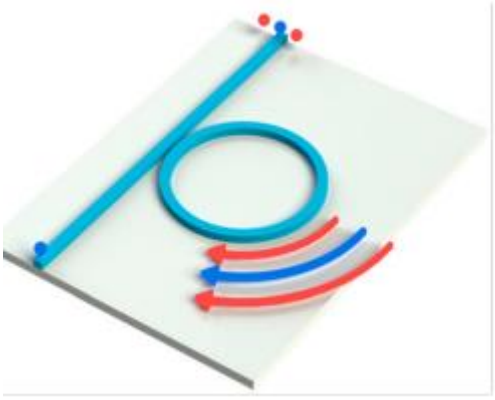

Figure 4 A diagram of a ring resonator to produce signal and idler states [3].

The number of resonant frequencies corresponds to the number of defect cavities forming the ring and it is from this set of frequencies that the idler, pump, and signal frequencies will be identified for SFWM.

3 Design Goals

By combining the advantageous features of ring resonators and photonic crystal cavities, this project aims to design a novel photonic crystal cavity ring resonator system, specifically focusing on multi-defect systems motivated by the structure of a micro-ring resonator (MRR). Using Lumerical and MATLAB simulations, we aim to optimize a coupled-cavity waveguide (CCW) linked to a ring resonator-like structure formed by defects in the photonic crystal slab (Figure 5). This configuration is expected to generate entangled squeezed states of light (see Appendix B), known as two-mode continuous-variable cluster states, with potential applications in universal quantum computation [7]. The project is focused on maximizing entangled squeezed light generation while minimizing losses by creating an ideal environment for SFWM, exclusively through a coupled-cavity ring resonator on a photonic crystal chip. Alternative approaches are considered beyond the scope of this project. These goals and constraints are summarized succinctly in Table 2.

Table 2 A brief overview of goals and constraints for the design of this project.

Goals	Constraints
Optimize mode frequency spacing	Semiconductor photonic crystal slab
Maximize nonlinear mode overlap	Square lattice of airholes
Maximize Q	Coupled-cavity ring resonator structure

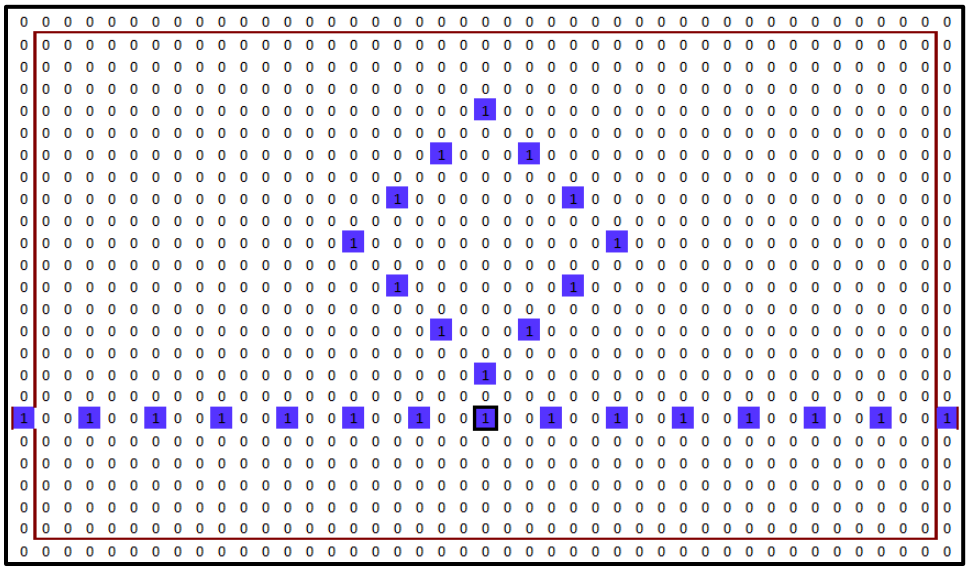

Figure 5 A schematic of a coupled-cavity ring resonator side-coupled to a CCW on a photonic crystal slab.

4 Design Process

Design and testing for this project was performed entirely in simulation. This was the most efficient method to quickly test many different preliminary designs. Simulations were performed in MATLAB using a tight binding toolbox and code for this task developed by Dylan Van Eeden, a PhD Candidate supervised by Prof. Dignam.

This program calculates the resonant modes of a specified coupled-cavity ring structure and generates a matrix that represents the eigenmodes associated with each resonant frequency in every cavity. Since the number of resonant modes is equal to the number of cavities in the ring, a ring constructed from 16 cavities for example, will result in a 16 x 16 matrix of eigenmodes.

The code takes as it's input a grid describing a photonic crystal architecture. An example of this architecture is shown in Figure 6.

This sheet represents a photonic crystal slab as indicated by the red borders. The blue squares represent defect cavities in the lattice structure. Simulations were performed by creating unique ring configurations formed by the defect cavities. The code implements TB, to simulate the interactions of the electric fields with the defect cavities.

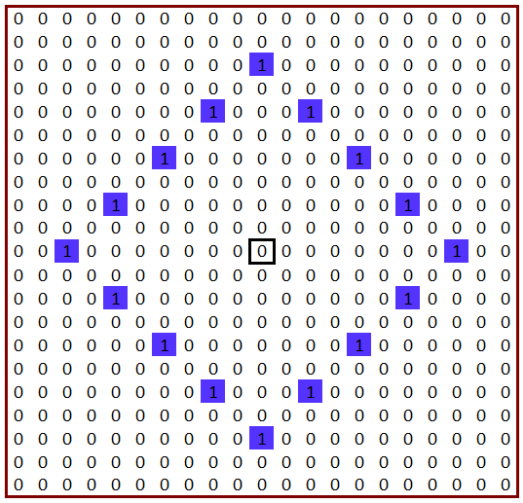

Figure 6 A ring resonator constructed on a photonic crystal slab from defects in a lattice of airholes.

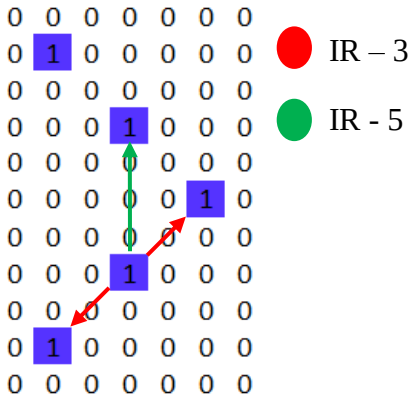

Figure 7 An illustration of the cavities considered based on interaction radius (IR). The corner adjacent cavities across from each other sit within an IR of 5.

Initial simulations were performed with an interaction radius (IR) of 3 cavity widths. This radius is large enough to consider the nearest neighbours around a given cavity. After an initial exploration was completed, this radius was expanded to 5. The primary effect of this expansion is on the cavities located one off the corner, which are now influenced by the cavity across the

corner from them. This is illustrated in Figure 7. This was done to test the model under less symmetrical conditions and was the method employed for all results that follow unless otherwise stated.

The lattice constant - the distance between the centers of adjacent cavities - is 480 nm. The void radius – the size of the cavities themselves – is 192 nm. The lattice constant was held constant throughout testing as was the void radius, while the radius for the defects in the ring was varied from 36 nm iteratively up to 127 nm.

Ring structures containing 8 + 4n cavities were found to exhibit a promising symmetry in the tight binding dispersion to satisfy the desired result of Eq. (7). For example, a ring with 8 cavities yields:

$$k_m d = \left\{-\frac{3\pi}{4}, -\frac{\pi}{2}, -\frac{\pi}{4}, 0, \frac{\pi}{4}, \frac{\pi}{2}, \frac{3\pi}{4}, \pi\right\} \tag{8}$$

Where $\frac{\pi}{4}, \frac{\pi}{2}$ and $\frac{3\pi}{4}$ satisfies Eq. (7).

Additionally, by choosing a pump frequency located at an inflection point on the tight binding dispersion relation, it is expected that signal and idler frequencies can be generated symmetrically on either side of the pump frequency. This is expected to yield the best phase matching conditions ensuring efficient energy transfer between interacting waves. This concept is illustrated in Figure 8.

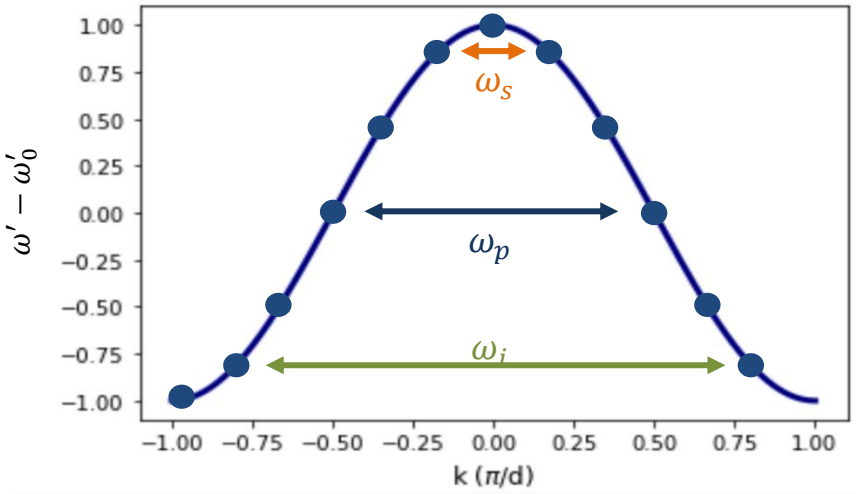

Figure 8 An example of a frequency combination that would provide ideal phase matching conditions.

5 Models and Simulations

Several cavity structures were constructed, and their resonant modes identified through simulation in MATLAB. A variety of cavity configurations were examined including ones which were dense, sparse, stretched, and askew as shown in Figures 9 and 10.

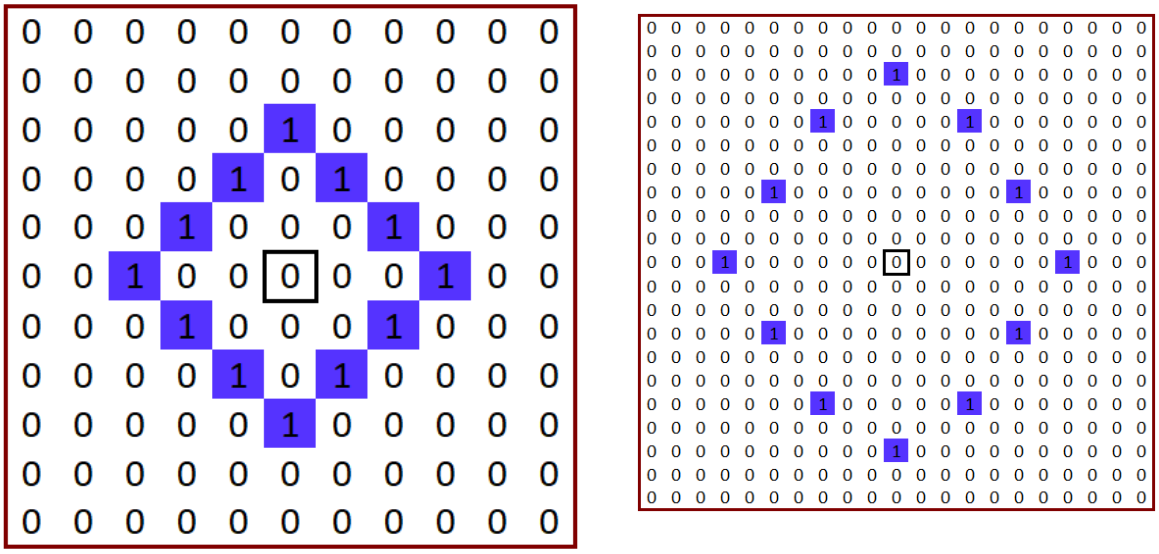

Figure 9 A dense 12-cavity ring (left) and a sparse 12-cavity ring (right).

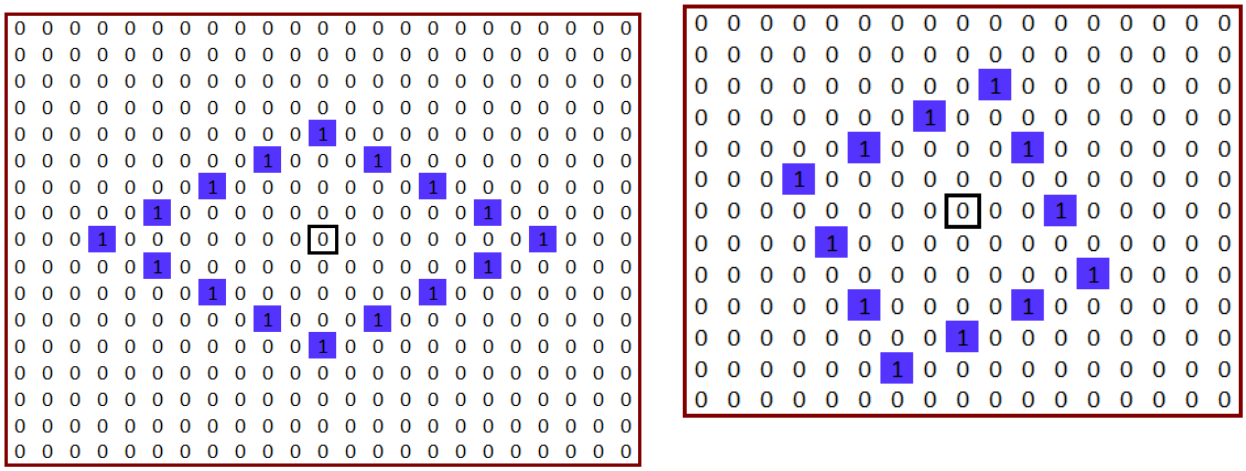

Figure 10 A stretched 16-cavity ring (left) and an askew 12-cavity ring (right).

Each of these structures yielded an array of complex resonant frequencies. We implemented a novel program in Python to analyze the resonant mode frequencies for the most optimal configurations adhering to Eq. (5). The configurations which yielded the most promising results were the uniformly doubly spaced rings – particularly of 16 and 24 cavities – as shown in Figures 11 and 12.

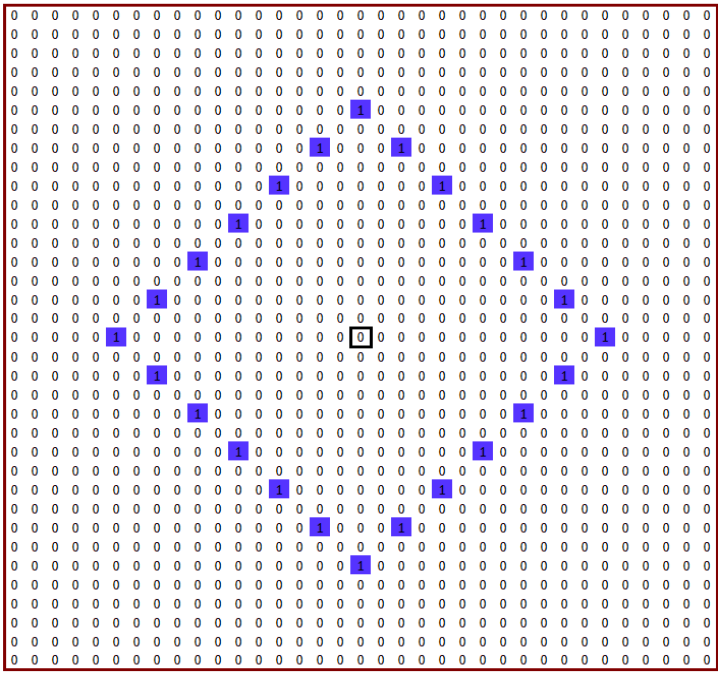

Figure 11 A uniformly doubly spaced 24-cavity ring.

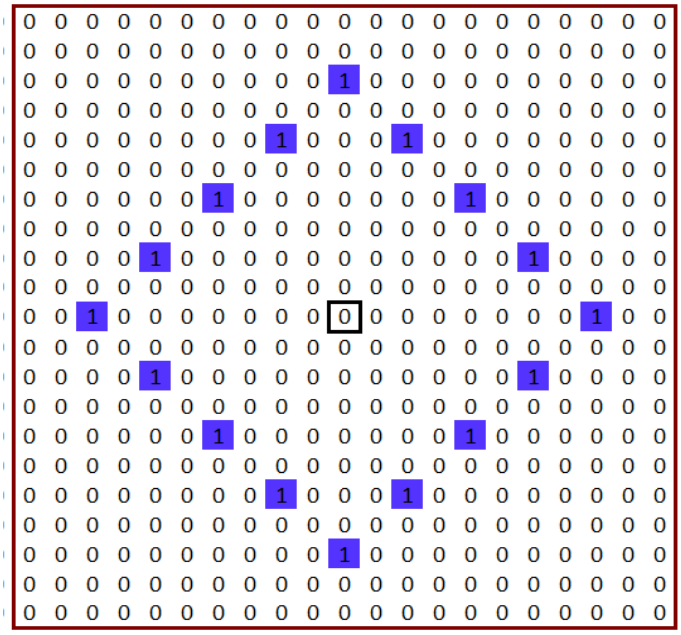

Figure 12 A uniformly doubly spaced 16-cavity ring.

6 Design Metrics

6.1 Mode Frequency Spacing

Frequency sets such as the one shown in Table 3 were analyzed to find a pair of frequencies that are equidistant from a central frequency so as to satisfy Eq. (5). The goal was to maximize separation from the chosen central frequency, while minimizing the relative difference in separations from the central frequency. By increasing the separation between frequencies, we should reduce contamination of the signal and idler frequencies by the pump frequency. We track the average separation between the signal and idler frequencies with respect to the pump frequency as:

$$\delta_{avg} = \frac{\omega_s' - \omega_i'}{2} \tag{9}$$

This represents the average separation between ω_s' and ω_i' relative to ω_p'. This term will be referred to as the average separation and a higher average separation indicates a more favourable configuration.

Another factor that needed to be considered in the design of the ring was the width of the Lorentzian modes for the resonant frequencies. Since the relative separation – the difference between $\omega_s' - \omega_p'$ and $\omega_p' - \omega_i'$ – is non-zero in each of these configurations, we aim to maximize the SFWM process by minimizing the ratio of the relative separation and the width of the Lorentzian modes. The full width at half maximum (FWHM) of a given complex frequency is given by twice the imaginary portion of the frequency (see Figure 13) [8].

$$FWHM = 2\omega'' \tag{10}$$

To measure this design goal, we have defined a metric called the O-score, which is given by:

$$O - score = \frac{\left(\omega_s' - \omega_p'\right) - \left(\omega_p' - \omega_i'\right)}{\frac{\omega_i'' + \omega_p'' + \omega_p''}{3}} \tag{11}$$

This represents the degree to which the Lorentzian distributions of the frequencies overlap in order to satisfy Eq. (5).

A lower O-score indicates a more favourable configuration and an O-score > 2 indicates a configuration that is entirely unconducive to SFWM as there will be no overlap between the FWMH of the Lorentzian curves.

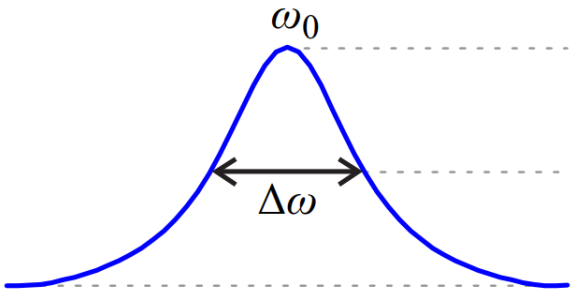

Figure 13 An illustration of a frequency mode characterized by a Lorentzian line shape. Maximum value and FWHM bandwidth are clearly marked [1].

The real part of ω gives the resonant frequency, while the imaginary part describes the energy leakage out of the associated defect mode [5]. The quality factor for these modes is then given by [8]:

$$Q = \frac{\omega_0}{\Delta\omega} = \frac{\omega'}{2\omega''} \tag{12}$$

The higher the quality factor, the greater the coherence of the resonant modes, indicating lower energy dissipation and better confinement of light [9].

6.2 Nonlinear Mode Overlap

In addition to resonant frequencies, each frequency has an eigenmode corresponding to a standing wave pattern that can exist within the coupled-cavity system. When two eigenmodes have the same frequency, these are called degenerate modes. The combination of these degenerate modes should itself be an eigenmode of the discrete translation operator, $\hat{T}$, which translates a mode by a defect period:

$$\hat{T}N_T = \lambda N_T \tag{13}$$

Where N_T is given by:

$$N_T = N_1\alpha_1 + N_2\alpha_2 \tag{14}$$

Where N_1 and N_2 are the degenerate eigenmodes and α_1 and α_2 are complex variational parameters which satisfy the relationship:

$$|\alpha_1|^2 + |\alpha_2|^2 = 1 \tag{15}$$

Each eigenmode is given by the equation:

$$N_j = \sum_n V_{jn} M_n(r), \qquad j = \{1, 2\} \tag{16}$$

Where M_n are the individual defect modes obtained through simulation in Lumerical (see Appendix A), and V_{jn} are normalized coefficients, called expansion coefficients, relating the modes of the individual defects to the modes of the system[1]. Using the Rayleigh-Ritz theorem, and minimizing $\langle\hat{T}\rangle$ with respect to α_1 and α_2, yields another eigenvalue problem:

$$M\alpha = \lambda\alpha \tag{17}$$

Where M is given by:

$$M = \begin{pmatrix} \sum_{q=1}^{N} V_{1,q}^* V_{1,(n-1)} & \sum_{q=1}^{N} V_{1,q}^* V_{2,(n-1)} \\ \sum_{q=1}^{N} V_{2,q}^* V_{1,(n-1)} & \sum_{q=1}^{N} V_{2,q}^* V_{2,(n-1)} \end{pmatrix} \tag{18}$$

And V_1 and V_2 represent the degenerate eigenmodes in the q'th cavity in an N-cavity ring. Solving this problem yields a set of 2 eigenvectors for each degenerate mode. We select the

[1] For a detailed derivation of the V_{jn} terms, the interested reader is referred to [5] and [6].

eigenvector whose eigenvalue corresponds to a positive wave vector (the eigenvalue with a positive argument) to obtain a physically meaningful solution. These linear combinations of degenerate modes can then be used to determine the non-linear optical interaction parameter χ which describes the degree to which SFWM is allowed to occur [5]:

$$\chi \cong \sum_{q=1}^{N} \left(V_q^p\right)^2 V_q^{s^*} V_q^{i^*} \tag{19}$$

Where each product in the summation is computed on the eigenmodes of the q^{th} cavity in the ring. This parameter is maximized when all 3 modes are large in the same cavities. From NNTB we obtain the expression for the expansion coefficients [6]:

$$V_q = \frac{e^{ikqd}}{\sqrt{N}} \tag{20}$$

Where d is the spatial periodicity given by the lattice constant. We expect a result close to this for a slightly expanded interaction radius as well. The value of χ in an N-cavity ring can thus be approximated by:

$$\chi \cong \frac{1}{N^2} \sum_{q=1}^{N} e^{i\Delta kqd} \tag{21}$$

Where:

$$\Delta \mathrm{k} = 2k_p - k_s - k_i \tag{22}$$

The maximum value of χ is given when $\Delta k = 0$ as:

$$\chi \cong \frac{1}{N} \tag{23}$$

7 Results

The most favourable frequency triplets for various configurations, all of which were uniformly doubly spaced, and the associated performance metrics are captured in Table 3.

Table 3 Resonant frequencies and performance metrics for various rings. The frequencies are scaled by the quotient of the lattice constant (480 nm) and the speed of light. Favourable O-scores are marked in green while unfavourable ones are marked in red.

# Cavities	r (nm)	ω_i' [a/c]	ω_p' [a/c]	ω_s' [a/c]	δ_{avg}	O-score
28	96	0.308837	0.310071	0.311314	0.00124	0.9153
24	127	0.316216	0.317603	0.318983	0.00138	0.6316
24	109	0.311161	0.312348	0.313533	0.00119	0.3141
24	103	0.311030	0.311568	0.312102	0.00054	0.5908
24	100	0.309366	0.310175	0.310986	0.00081	0.2247
24	96	0.308788	0.309945	0.311102	0.00116	0.0337
24	36	0.304618	0.305388	0.306172	0.00078	1.7100
20	96	0.309985	0.310785	0.311590	0.00080	0.2738
20	36	0.303302	0.304186	0.305078	0.00089	1.0100
16	96	0.308826	0.310280	0.311734	0.00145	0.0190
16	92	0.308240	0.309682	0.311116	0.00144	1.0388
16	36	0.304170	0.304880	0.305600	0.00072	1.3123
12	96	0.311065	0.311487	0.311926	0.00043	1.8012
12	68	0.306788	0.307163	0.307552	0.00038	1.6813
8	96	0.310280	0.310884	0.311563	0.00064	8.2200

Ring performance was investigated at increasing ring size, while holding the defect radius constant at 96 nm. The performance metrics for these tests are charted in Figure 14.

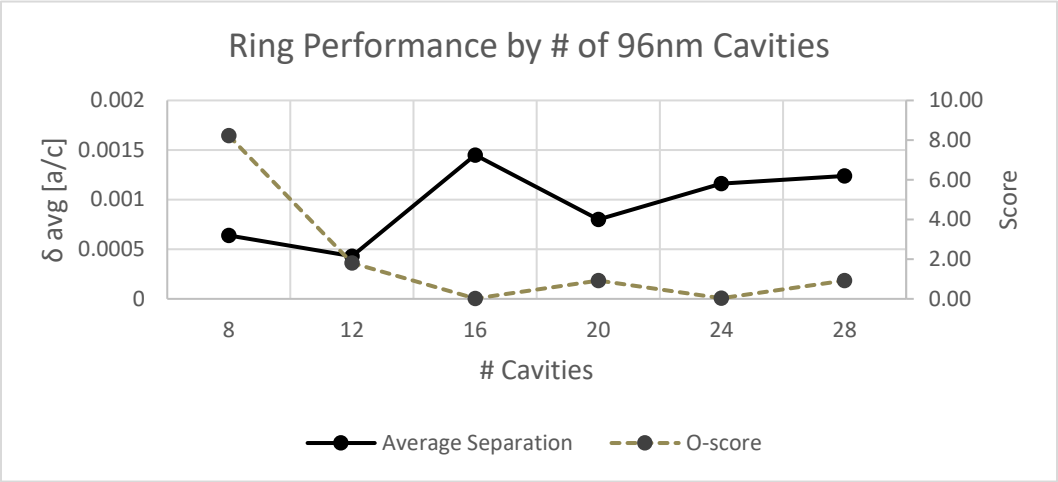

Figure 14 An analysis of performance by the # of cavities forming a uniformly doubly spaced ring for a 96 nm defect radius.

We also examined the effect of increasing the defect radius for a given structure. This is charted for a 24-cavity ring in Figure 15.

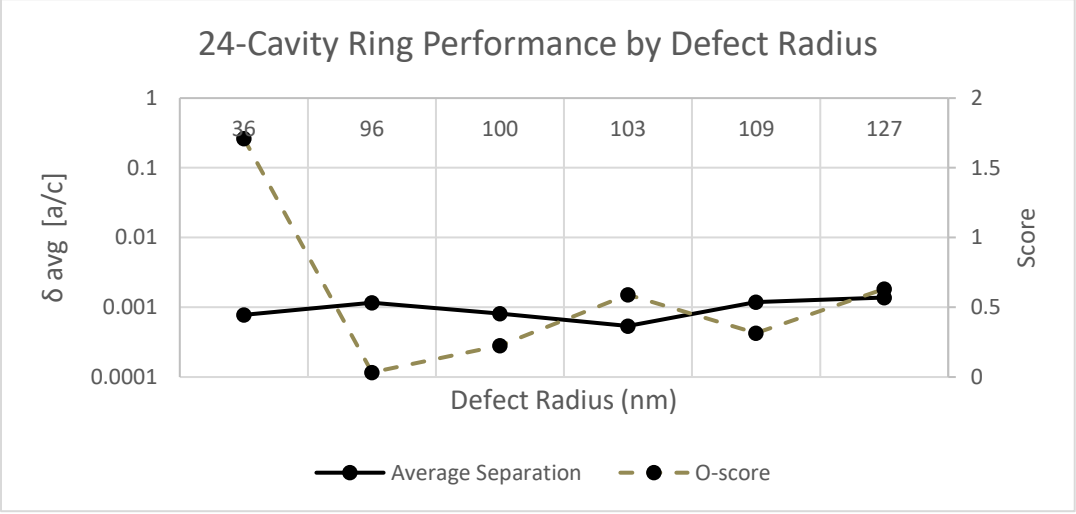

Figure 15 An analysis of performance by the radius of cavities forming a uniformly doubly spaced 24-cavity ring.

Table 3 indicates many configurations which exhibit optimal mode frequency spacing for SFWM. However, these combinations must also be examined for maximal nonlinear mode overlap. That is, the eigenmodes associated with each frequency must be large in the same cavities within the ring, otherwise there will be no environment suitable for SFWM. Table 4 shows the nonlinear optical interaction parameter, χ, calculated using Eq. (19) for the promising

ring configurations established during mode frequency analysis. Overlap efficiency is calculated by $\frac{\chi}{N}$ where N is the number of cavities in the ring as per Eq (23). Δk is calculated by using the argument of the eigenvalues for the three degenerate modes in Eq. (22).

Table 4 The most favourable frequency triplets and their associated nonlinear mode overlap.

# Cavities	r (nm)	ω_i' [a/c]	ω_p' [a/c]	ω_s' [a/c]	χ	Overlap Efficiency	Δk
24	100	0.309366	0.310175	0.310986	2.63E-3	6.31%	-0.0054
24	96	0.308788	0.309945	0.311102	9.19E-15	2.2E-13%	-1.35
16	96	0.308826	0.310280	0.311734	1.12E-12	1.8E-11%	-0.406

Though the frequency triplets for the 96 nm configurations exhibited the best mode frequency spacing, they do not align symmetrically on the tight binding dispersion relation. This means that there are an unequal number of points between each frequency and the pump frequency. The only configuration examined which exhibited optimal mode frequency spacing and satisfied this criterion was the 24-cavity ring with a defect radius of 100 nm. To confirm this theory, frequencies from a 12-cavity ring in a NNTB model were selected which align symmetrically on the dispersion relation. Additionally, each pair of frequencies was perfectly degenerate. The resulting χ was 99.988% as captured in Table 5. This configuration would not work for the final design however, because the mode frequency spacing is very poor.

Table 5 A ring configuration which exhibits near-perfect nonlinear mode overlap at the expense of optimal mode frequency spacing.

# Cavities	r (nm)	ω_i' [a/c]	ω_p' [a/c]	ω_s' [a/c]	O-score	χ	Overlap Efficiency	Δk
12	96	0.308997	0.310277	0.311882	35.501	0.0833	99.988%	-3.32E-5

8 Final Design

The design which was found to best balance both optimal mode frequency spacing and nonlinear mode overlap was a uniformly doubly spaced 24-cavity ring with a defect radius of 100 nm. This configuration is shown in Figure 16.

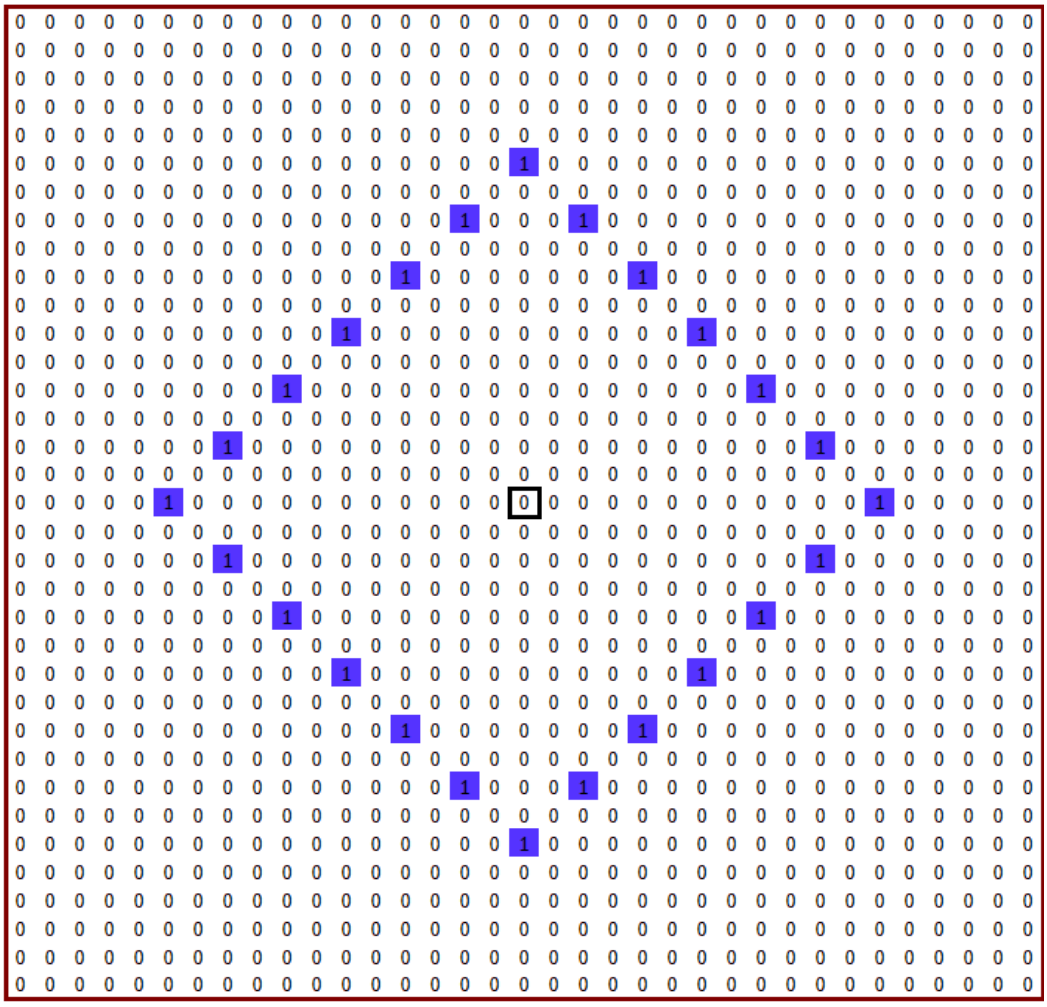

Figure 16 The coupled-cavity ring configuration which yielded the best performance; a uniformly doubly spaced 24-cavity ring.

Table 6 captures the complex resonant frequencies in ascending order along with their quality factors where the idler, pump and signal frequencies are highlighted green, blue, and orange respectively. The pattern of degenerate pairs predicted by the tight binding dispersion is denoted by the alternating white and grey rows. The degeneracy exhibited, however, is imperfect under an expanded interaction radius. The performance metrics for this design are captured in Table 7.

Table 6 The resonant frequencies for the 24-cavity ring with defect radius of 100 nm.

ω' [a/c]	ω'' [a/c]	Q
0.308641	-9.13E-06	16896
0.308686	-9.12E-06	16927
0.308686	-9.12E-06	16927
0.308766	-9.09E-06	16984
0.308954	-9.03E-06	17099
0.309124	-8.98E-06	17219
0.309124	-8.98E-06	17219
0.309366	-8.90E-06	17388
0.309541	-8.84E-06	17508
0.309847	-8.74E-06	17728
0.309847	-8.74E-06	12728
0.310175	-8.63E-06	17966
0.310380	-8.56E-06	18122
0.310705	-8.46E-06	18365
0.310705	-8.46E-06	18365
0.310986	-8.37E-06	18577
0.311229	-8.29E-06	18781
0.311436	-8.22E-06	18940
0.311436	-8.22E-06	18940
0.311579	-8.18E-06	19050
0.311820	-8.09E-06	19266
0.311877	-8.08E-06	19307
0.311877	-8.08E-06	19307
0.311912	-8.07E-06	19335

Table 7 The idler, pump, and signal frequencies for the best performing ring along with the relevant performance metrics. The quality factors of the 6 frequencies were averaged to calculate Q_{avg}.

# Cavities	a_0 (nm)	ω_i' [a/c]	ω_p' [a/c]	ω_s' [a/c]	δ_{avg}	O-score	$\lvert\chi\rvert$	Overlap Efficiency	Q_{avg}
24	100	0.309366	0.310175	0.310986	0.000810	0.225	0.002629	6.31%	18057
		0.309541	0.310380	0.311229	0.000844	1.205			

9 Discussion

This exploration of coupled-cavity ring resonators yielded valuable results which confirmed the theoretical framework which guided the design goals. The final design was one in which:

1. The pump frequency was at the inflection point on the curve given by the tight binding dispersion.
2. Both the signal and idler modes were nearly equidistant in k-space from the pump frequency.
3. The signal and idler frequencies were nearly equidistant from the pump frequency.
4. All 3 modes were treated as degenerate for the calculation of χ.

The effectiveness of equal separation in k-space was confirmed as the configurations with smaller values for Δk exhibited much better spatial overlap. We also observed that three perfectly degenerate modes in a NNTB model with $\Delta k = 3.32 * 10^{-5}$ exhibited 99.988% overlap efficiency in the calculation of χ.

Average separation and O-score exhibited some inverse correlation as can be observed in Figures 14 and 15. These figures did not indicate a discernable trend between ring performance and ring size or defect radius, though some configurations did perform markedly better than others. Defect radii in the range of 96 - 109 nm consistently performed better across ring configurations. For a lattice with a void radius of 192 nm, this represents defects which are 50% - 56.8% the size of the void radius.

The 24-cavity configuration selected for the final design spans 25 cavities in either direction. This represents a ring radius of 2.4 μm. This is much smaller than the radius for a small waveguide ring resonator, which is typically on the order of 100-10000 μm [10] [11]. The coupled-cavity ring is therefore only ~2% the size of a typical waveguide ring resonator.

The nonlinear optical interaction result of 0.002629 with an overlap efficiency of 6.31% was less than we would hope for practical implementation but may be ameliorated with further exploration of configurations with a focus on perfectly degenerate mode frequencies centered around the inflection point given by the tight binding dispersion.

The mode frequencies in the final design exhibited an average quality factor of 18057 which is much smaller than what can be achieved by waveguide ring resonators. The quality factor was not observed to be very sensitive to changes in ring configuration, consistently scoring on the order of 10^4. The imaginary parts of the mode frequencies were consistently on the order of 10^{-6} - 10^{-5}. This is much lower than the quality factors achieved in waveguide ring resonators as high as 10^8 [11].

Future work on this project should include optimizing the ring configuration by maximizing the mode frequency spacing and the nonlinear mode overlap with a focus specifically on triplets centered around the inflection point given by the tight binding dispersion. We may improve the design process by developing a program to autonomously scan the mode frequencies and eigenmodes for the optimal configuration across defect radii for a given ring. Future work should also include expanding upon the comparisons to the waveguide ring resonators by including all factors affecting squeezed light generation to quantify a comprehensive SFWM efficiency metric as a function of ring radius. Lastly, in order to determine the viability of practical implementation, the sensitivity of ring performance to manufacturing defects should be examined.

10 Conclusion

This report detailed the design process of a novel photonic crystal cavity ring resonator system aimed at maximizing the generation of entangled squeezed light. Through a combination of theoretical analysis, and simulation in Lumerical and MATLAB, various configurations of coupled-cavity ring resonators were explored, with a focus on optimizing mode frequency spacing, nonlinear mode overlap, and quality factor.

The most optimal configurations were found to be ones in which the signal and idler frequencies were equally spaced around the pump frequency which sat at the inflection point given by the tight binding dispersion relation. Notably, a uniformly doubly spaced 24-cavity ring with a defect radius of 100 nm emerged as the most promising design, achieving an average mode frequency separation of 0.000827, an average O-score of 0.715, and 6.31% nonlinear mode overlap efficiency. This design not only showcases the potential for efficient generation of entangled squeezed states but also highlights the importance of careful parameter optimization in achieving desired performance. Further experimentation with ring configurations of varying ring size and cavity defect size is essential for optimizing the design and realizing practical viability.

Moving forward, optimization of these theoretical findings and an examination of sensitivity to manufacturing defects will be crucial in assessing the practical viability of the proposed design. Moreover, further research into refining fabrication techniques and addressing environmental considerations will be essential for realizing the full potential of such a design as it applies to quantum computing technologies. Overall, this study contributes to the ongoing advancement of nonlinear optics applications in quantum computing, particularly in the realm of photonic crystal cavity ring resonator systems for generating squeezed light, while also encouraging further scientific inquiry into the challenges that lie ahead.

Appendix A. Statement of Work

This appendix provides a detailed overview of the work completed in relation to the thesis project during the fall and winter terms. No work related to this project was completed prior to September 1st.

Fall Term Work (September - December):

- Completed a comprehensive review of relevant literature to establish a theoretical framework.
- Formulated research hypotheses and objectives in collaboration with the thesis advisor.
- Set up a simulation environment to accommodate the large memory requirements for testing.

Winter Term Work (January - April):

- Simulated various ring configurations in MATLAB.
- Wrote a unique program in Python to identify the optimal frequency triplets given a set of resonant frequencies.
- Developed theoretical models in collaboration with the thesis advisor to explain observed phenomena, address mode degeneracy and calculate the non-linear optical interaction parameter.
- Drafted the findings from the project into a thesis report.

Collaborations:

- Engaged in regular consultations with the thesis advisor, Prof. Dignam, to refine research methodologies and interpret results effectively.
- Used an existing code from Dylan Van Eden, a PhD Candidate supervised by Prof. Dignam, to simulate the resonant modes in MATLAB. Also used single defect field profiles created by Dylan in Lumerical as the defect cavity inputs in MATLAB.

Appendix B. Two-Mode Squeezed States

Similar to Heisenberg uncertainty, it can be shown that conjugate observables for light satisfy the relation:

$$\Delta X \Delta Y \geq 1 \tag{2}$$

where the dimensionless quadrature operators ΔX and ΔY are given by

$$\Delta X = b + b^{\dagger} \tag{3}$$

and

$$\Delta Y = -i(b - b^{\dagger}). \tag{4}$$

The b operators are related to the quantum creation and annihilation operators. By applying the squeezing operator

$$S(\xi) = exp\left(\frac{1}{2}(\xi^{*}b^{2} - \xi b^{\dagger 2})\right) \tag{5}$$

a squeezed state is produced where the uncertainty in the quadratures can be interchangeably represented as

$$(\Delta X)^{2} = e^{-2u} \tag{6}$$

and

$$(\Delta Y)^{2} = e^{+2u}. \tag{7}$$

In this case the state is "squeezed" in X and "stretched" in Y as illustrated in Figure 17.

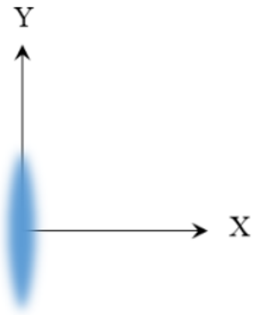

Figure 17 An illustration depicting the squeezing of the uncertainty in the X quadrature.

For two-mode entangled states, the squeezing can be represented as

$$\langle[\Delta(X_1 - X_2)]^2\rangle = 2e^{-2u} \tag{8}$$

and

$$\langle[\Delta(Y_1 + Y_2)]^2\rangle = 2e^{-2u} \tag{9}$$

where the subscripts denote the entangled state for the corresponding quadrature. In this case one mode will be X-squeezed and the other, Y-squeezed. The states are also entangled as a measurement of a quadrature in one mode narrows the range of likely measurements in the corresponding quadrature in the other mode.

For a more complete derivation of entangled squeezed states of light, refer to [12]. Refer to [6] for more information on entangled squeezed states of light in lossy coupled resonator optical waveguides.

References

[1] T. Ralph, "Quantum Optical Systems for the Implementation of Quantum Information Processing," *Reports on Progress in Physcs,* vol. 69, no. 4, 2006.

[2] R. W. Boyd, Nonlinear Optics, 4th ed., Academic Press, 2020.

[3] C. Vendromin, "Nonlinear Optical Generation of Multimode Entangled Squeezed Thermal States," 2023.

[4] J. E. Heebner, R. Grover and T. A. Ibrahim, Optical Microresonators: Theory, Fabrication and Applications, Springer, 2008.

[5] D. Van Eeden, "Nonlinear Generation of Quantum States of Light in Lossy Coupled-Resonator Systems," 2022.

[6] S. Hossein and M. M. Dignam, "Squeezed state evolution and entanglement in lossy coupled resonator optical waveguides," *Physical Review A,* vol. 97, 2018.

[7] N. C. Menicucci, P. van Loock, M. Gu, C. Weedbrook, T. C. Ralph and M. A. Nielsen, "Universal Quantum Computation with Continuous-Variable Cluster States," *Physical Review Letters,* vol. 97, no. 11, 2006.

[8] T. Christopoulos, O. Tsilipakos, G. Sinatkas and E. E. Kriezes, "On the calculation of the quality factor in contemporary photonic resonant structures," *Optics Express,* vol. 27, no. 10, 2019.

[9] D. P. Fussell and M. M. Dignam, "Engineering the quality factors of coupled-cavity modes in photonic crystal slabs," *Applied Physics Letter,* vol. 90, 2007.

[10] N. Gruhler and W. H. P. Pernice, "High-quality Si3N4 circuits as a platform for graphene-based nanophotonic devices," *Optics Express,* vol. 21, no. 25, 2013.

[11] M. W. Puckett, K. Liu and N. Chauhan, "422 Million intrinsic quality factor planar integrated all-waveguide resonator with sub-MHz linewidth," *Nat Commun,* vol. 12, no. 934, 2021.

[12] C. G. Gerry and P. Knight, Introductory quantum optics, Cambridge: Cambridge University Press, 2005.

[13] X. Youg, R. K. Lee and A. Yariv, "Propagation and second-harmonic generation of electromagnetic waves in a coupled-resonator optical waveguide," *Journal of the Optical Society of America B,* vol. 17, no. 3, 2000.